Applied Thermal Engineering 116 (2017) 445–455

Contents lists available at ScienceDirect

Applied Thermal Engineering

journal homepage: www.elsevier.com/locate/apthermeng

Research Paper

Performance analysis of a novel compact air-air heat exchanger for aircraft gas turbine engine using LMTD method

Haiwang Li [a,b,c], Haoran Huang [c], Guoqiang Xu [a,b], Jie Wen [a,b,*], Hongwei Wu [d]

[a] National Key Laboratory of Science and Technology on Aero Engines Aero-thermodynamics, Beihang University, Beijing 100191, China
[b] The Collaborative Innovation Center for Advanced Aero-Engine of China, Beihang University, Beijing 100191, China
[c] Aircraft/Engine Integrated System Safety Beijing Key Laboratory, Beihang University, Beijing 100191, China
[d] Department of Mechanical and Construction Engineering, Faculty of Engineering and Environment, Northumbria University, Newcastle upon Tyne NE1 8ST, United Kingdom

HIGHLIGHTS

- A new type of compact cross-flow snake tube heat exchanger was designed and optimized.
- A new hybrid cooling system used in aero-engine is introduced.
- Experimental results prove that the LMTD method is reliable for compact heat exchanger design and calculation.
- An empirical relationship for outside heat transfer of compact snake tube heat exchanger is developed.

ARTICLE INFO

Article history:
Received 28 September 2016
Revised 21 November 2016
Accepted 2 January 2017
Available online 1 February 2017

ABSTRACT

In this article, a new compact cross-flow air-air heat exchanger is designed using logarithmic mean temperature difference method (LMTD) and its performance is experimentally investigated with optimized structure. The designed heat exchanger weights 2.04 kg which is able to cool the high temperature air from high pressure compressor in aero engine for more than 200 K (in certain cases) in a very limited space by using the coolant air from bypass duct. A comparison between calculated results and the obtained experimental data is presented and discussed. Results show good agreement between the current calculations and experimental data. It also reveals that the present design method is proved to be relatively accurate in predicting the performance of the compact air-air heat exchanger for all the investigated structures. What's more, a new empirical correlation for the outside heat transfer coefficient is established using Wilson plot method in the current study. The correlation will be helpful for the researchers to design new air-air heat exchangers.

1. Introduction

The inlet temperature of modern gas turbine engines has been increased to achieve higher thermal efficiency. Current turbine inlet temperatures are approaching 2000 K, which is far beyond the allowable metal temperatures. As the material development of coatings and base material reach a culminating point, further increases in turbine inlet temperatures can only come from highly sophisticated cooling techniques [1,2]. Various cooling technologies including internal convective cooling and external film cooling have been successfully employed to cool high temperature components for the last half century. It is apparent that internal convective cooling is insufficient to maintain the blade at the required temperature and, thus, film cooling is required and becomes one of the most effective and widely used cooling methods to gas turbine blade to prevent thermal failure in extremely high temperature operations [3]. A comprehensive compilation of the available advanced cooling techniques used in the gas turbine industry has been encapsulated by Han et al. [4] in their book.

Though cooling is an effective way to enable higher inlet temperatures, an adequate cooling is challenging due to geometric constraints in combination with aerodynamic demands [5]. Besides, efficiency considerations demand effective cooling to be accomplished with minimum amount of cooling air which conflict with the application of film cooling that large cooling air are required. Since the coolant that facilitates the film cooling is extracted from the compressor, poor management of the cooling air can be otherwise detrimental to the engine overall efficiency. Furthermore, the cooling air capacity becomes more limited due to the increase in its stagnation temperature. Consequently, when

* Corresponding author at: National Key Laboratory of Science and Technology on Aero Engines Aero-thermodynamics, Beihang University, Beijing 100191, China.
E-mail address: 09620@buaa.edu.cn (J. Wen).

http://dx.doi.org/10.1016/j.applthermaleng.2017.01.003
1359-4311/

Nomenclature

A_o	outside heat transfer area (m^2)
c_l	inlet section correction factor
c_p	isobaric specific heat capacity (kJ kg^{-1} K^{-1})
c_r	bending tube correction factor
d	diameter (m)
f_i	fanning friction factor
h_i	inside heat transfer coefficient (W m^{-2} K^{-1})
h_o	outside heat transfer coefficient (W m^{-2} K^{-1})
K_o	outside overall heat transfer coefficient (W m^{-2} K^{-1})
L	total length (m)
$\dot{m}$	mass flow (kg s)
N	number of tube rows
Δp_d	distance flow resistance (Pa)
Δp_N	flow resistance due to inlet and outlet pipe connection (Pa)
Δp_o	outside flow resistance (Pa)
Δp_r	flow resistance due to return flow (Pa)
Δp_t	total flow resistance (Pa)
Q	total heat transfer rate (W)
R	thermal resistance (K)
r	bending radius of tubes (m)
T	temperature (K)
ΔT_m	logarithmic mean temperature difference (K)
ΔT_{max}	the bigger one of $(T_{c,o} - T_{h,o})$ and $(T_{h,i} - T_{c,i})$ (K)
ΔT_{min}	the smaller one of $(T_{c,o} - T_{h,o})$ and $(T_{h,i} - T_{c,i})$ (K)
$\Delta T_{m,counter}$	logarithmic mean temperature difference when counter flow (K)
u	velocity (m s^{-1})
Z_t	number of tubes

Dimensionless quantity

Nu	Nusselt number
Pr	Prandtl number
Re	Reynolds number

Abbreviation

FHEX	finned-tube heat exchanger
HPC	high pressure compressor
LMTD	logarithmic mean temperature difference method

Greek symbols

φ	temperature difference correction factor
λ	thermal conductivity (W m^{-1} K^{-1})
ρ	density (kg m^3)
μ	dynamic viscosity (Pa s)
ϕ	correction factor of fluid viscosity

Subscripts

c	cold or cold side
exp	experimental
f	fluid
h	hot or hot side
i	inside or inlet
m	average
o	outside or outlet
s	stainless steel/fouling (thermal resistance)
t	total
ver	verification
w	wall

both internal and external film cooling are inadequate, there is still an urgent demand to seek a new design concept or optimal cooling techniques for better and more efficient cooling systems.

A convenient source of additional cooling capacity is the kerosene fuel carried on board the aircraft. The best performing option is to utilize the fuel as the primary heat sink due to its high capacity so that compressor bleed air is cooled with fuel in a nearby fuel-air heat exchanger, and then used to cool the hot engine components [6]. The successful implementation of this application can lead to the coolant quality is greatly improved on one hand, and the desired nebulization for further efficient combustion on the other hand. However, as the fuel absorbs heat from the wall, the fuel temperature can be increased beyond a certain high temperature. Due to aviation fuel is subject to high heat loads, it will lead to form unwanted surface/solid deposits, which can result in several effects that are detrimental to the aircraft fuel system and specifically in fuel nozzles [7,8]. Furthermore, the formation of coking will further reduce heat transfer by acting as an insulator on surfaces [9]. On the other hand, the fuel pressure is normally higher than the fuel critical pressure, thus, the fuel can become supercritical before injection into combustor [10,11]. Thus, the fuel thermodynamic and transport properties become very complex. As a consequence, the use of air-fuel heat exchanger only on the aero engine is restricted for its large size. A hybrid cooling system which consists of an air-air heat exchanger followed by an air-fuel heat exchanger, however, could overcome those disadvantages, as shown in Fig. 1. The air bled from the high pressure compressor will be cooled initially through bypass air and then further cooled by the fuel. In this way the coolant fuel temperature inside the air-fuel heat exchanger is able to be controlled at lower than 200 °C, and coke deposit speed under the temperature can be considered as very low. Since the air is cooled twice, the obtained cooling air can not only meet the cooling requirement of high heat-flux electronic components but also improve the combustion characteristics of the fuel. What's more, modular design method are applied in the hybrid cooling system, so the air-air heat exchanger, the air-fuel heat exchanger and tubes can be easily inspected and renewed even if the system encounters failure.

During literature surveys it was found that there were many research works investigated the air-side flow and heat transfer characteristics of finned tube and air-air heat exchangers. Kong et al. [12] carried a three-dimensional investigation to clarify the air-side flow and heat transfer performances of flat and slotted finned tube bundles and validated against experimental data. Their results showed that the finned tube bundles with slotted fins are superior to those with flat fins in heat transfer performance, but present a high pressure drop. Liu et al. [13] performed a numerical study on the enhancement of air-side heat transfer performance by using perforated fins for a finned-tube heat exchangers (FHEXs) with large fin pitches. It was concluded that an optimal perforation design can be obtained to realize maximum increase in the *j* factor for the perforated FHEX compared with those of the plate FHEX without perforations. Vafajoo et al. [14] developed a two-dimensional, compressible and turbulent flow for flue gas-air Chevron type plate heat exchangers. Their study showed that the bigger angle of the Chevron type plates resulted in 18% enhancement in the output air temperature as well as an increase in the resulting flue gas pressure drop of 63% in comparison with the plate heat exchanger. Zhang [15] carried out a combined numerical and experimental study on the flow maldistribution and thermal performance deterioration in cross-flow air to air heat exchangers. Results showed that when the channel pitch is below 2 mm, the flow distribution is quite homogeneous and the thermal deterioration due to flow maldistribution can be neglected. Whereas when

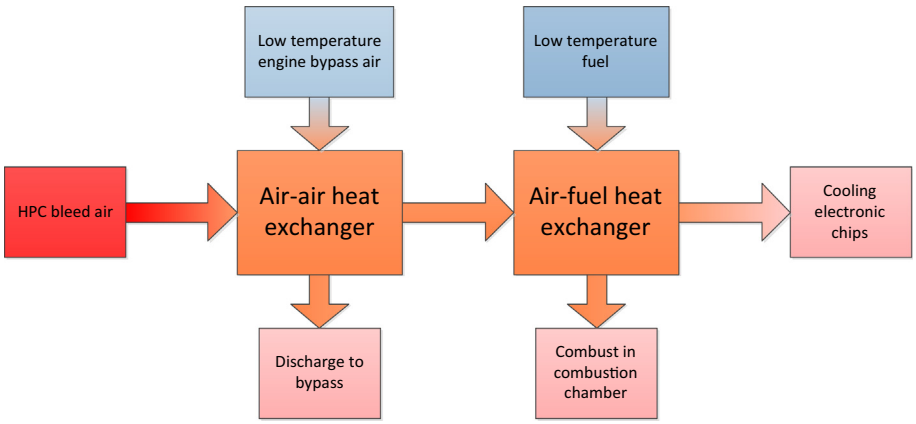

Fig. 1. The schematic diagram of a hybrid cooling system.

the channel pitch is larger than 2 mm, the maldistribution is quite large and a 10–20% thermal deterioration factor could be found. Vargas and Bejan [16] optimized the performance of air-air heat exchangers for airplane environmental control systems. Their results showed that the thermodynamic (constructed) optimization method of flow geometry illustrated in the paper is applicable to any systems that runs on the basis of a limited amount of fuel (exergy) installed onboard. Aristotle University of Thessaloniki and MTU Aero Engines also made many efforts on both experimental and numerical investigation of a new kind of air-air heat exchanger with U-shaped elliptic profiled tubes [17–20]. This heat exchanger allows the heat transfer between air from high pressure compressor and gas flow from turbine. By using oval tubes of staggered arrangement, the heat exchanger combines benefits from minimum aerodynamic pressure losses with high heat transfer effectiveness. Besides energy saving and effectiveness improvement, the heat exchanger can also reduce NOx emissions and noise levels, thanks to different combustion chamber conditions and to a high bypass ratio configuration.

Although many significant results on air-air heat exchanger have been already achieved by now, the application of air-air heat exchanger is still quite limited, especially for the cases in aero engine. As such, the present work aims to design and experimentally determine the performance of a compact air-air heat exchanger as well as acquire necessary data to provide support for the design of the cooling system.

2. Design and verification

2.1. Design

In the current work, the Logarithmic Mean Temperature Difference Method (LMTD) is applied to design the proposed air-air heat exchanger. This method was introduced in detail by Kay and Nedderman [21] and will not be repeated here. As it is usually the case, the total heat transfer rate (Q) can be determined as follow:

$$Q = \dot{m}_h c_{p_h}(T_{h,i} - T_{h,o}) = \dot{m}_c c_{pc}(T_{c,o} - T_{c,i}) \tag{1}$$

where the c_{p_h} and the c_{pc} can be determined using EES [22].

The logarithmic mean temperature difference for co-current flow and counter flow can be calculated easily. However, for the heat exchanger in this paper, fluid flow pattern is cross flow, so correction coefficient φ was introduced [23] and the fixed logarithmic mean temperature difference are as follow

$$\Delta T_m = \varphi * \Delta T_{m,counter} \tag{2}$$

For circular tubes, the overall heat transfer coefficient K_0 can be calculated by

$$\frac{1}{K_o} = \frac{1}{h_i}\frac{d_0}{d_i} + \frac{d_0}{2\lambda_s}\ln\left(\frac{d_o}{d_i}\right) + \frac{1}{h_o} \tag{3}$$

where the calculation of h_o and h_i is shown in Table 1.

Table 1
Heat transfer coefficient and flow resistance equation.

Section	Equation
Outside engine bypass air	Heat transfer coefficient $Nu_o = \frac{h_o d_o}{\lambda_o} = 0.27 Re_o^{0.63} Pr_o^{0.36}(Pr_o/Pr_{w,o})^{0.25}$ where $Re_o = \frac{\rho u_o d_o}{\mu}$, $Pr_o = \frac{c_{p_o}\mu_o}{\lambda_o}$, $Pr_{w,o} = \frac{c_{Pw,o}\mu_{w,o}}{\lambda_{w,o}}$, valid for $0.6 < Pr < 500$ and $1000 < Re < 200{,}000$ Flow resistance $\Delta p_o = 0.66 Re_o^{-0.2}\rho u_m^2(\mu/\mu_w)^{0.14}N$ where $Re_o = \frac{\rho u_m d_o}{\mu}$, valid for $100 < Re < 50{,}000$
Inside HPC bleed air	Heat transfer coefficient $Nu_i = \frac{h_i d_i}{\lambda_i} = 0.021 Re_i^{0.8} Pr_i^{0.45}(Pr_i/Pr_{w,i})^{0.25} c_l c_r$ where $Re_i = \frac{\rho u_i d_i}{\mu}$, $Pr_i = \frac{c_{p_i}\mu_i}{\lambda_i}$, $Pr_w = \frac{c_{Pw,i}\mu_{w,i}}{\lambda_{w,i}}$, considering inlet section effect and curved section effect, the coefficients $c_l = 1 + (\frac{d_i}{L})^{0.7}$ and $c_r = 1 + 1.77\frac{d_i}{r}$ is introduced, and the equation is valid for $0.6 < Pr < 700$ and $10{,}000 < Re < 1{,}750{,}000$ Flow resistance $\Delta p_t = \Delta p_d + \Delta p_r + \Delta p_N$ where $\Delta p_d = 4 f_i \frac{L}{d_i}\frac{\rho u_i^2}{2}\phi_i$ $\Delta p_r = 4\frac{\rho u_i^2}{2} Z_t \Delta p_N = 1.5\frac{\rho u_i^2}{2}$ In which $\phi_i = (\mu/\mu_w)^{-0.14}$ when $Re > 2100$, and $\phi_i = (\mu/\mu_w)^{-0.25}$ when $Re < 2100$, valid for $100 < Re < 50{,}000$

The heat transfer equation is defined as

$$Q = K_o A_o \Delta T_m \tag{4}$$

Combining Eqs. (1)–(4), the heat transfer area A_0 can be calculated, and then the structure of the heat exchanger can be completely determined. The calculated structure should be optimized in case the control parameters such as flow resistance, weight and volume requirement are not satisfied.

2.2. Verification

In this section, the heat transfer area is completely determined and the inlet temperatures on both hot side and cold side are given as well. The fluid temperature on either hot side or cold side is assumed initially, and the other side fluid temperature can be calculated by Eq. (1). Then ΔT_m, K_o and Q can be determined using Eqs. (2)–(4), respectively. Comparing, if the difference between the Q calculated by Eqs. (1) and (4) is not small enough, the inlet temperature should be reassumed until the difference is acceptable, or the heat exchanger should be re-designed.

Table 1 also lists the calculation of the outside and inside flow resistances [24].

3. Experimental apparatus and methods

The experimental study was conducted on a new heat exchanger test rig at the National Key Laboratory of Science and Technology on Aero-engines Aero-thermodynamics at Beihang University, China.

3.1. Test rig

The facility includes a high temperature air loop and a low temperature loop. These two loops provide high temperature air and low temperature air to simulate HPC bleed air (with high temperature) and bypass air (with low temperature) flow respectively. As shown in Fig. 2, the compressed air from air source is divided into two parts. In the high temperature air loop, the compressed air flows through a filter to remove impurities such as dusts. Then the air passes through flow control valve to control the flow rate with the desired value accurately by a thermal flow meter. The air stream is heated from room temperature to 500 K by an electric heater with the accuracy of ±1 K to simulate hot air from HPC. Exiting the heater, the air enters a 4 m long straight tube to provide uniform inlet flow for the air-air heat exchanger. Similar to the high temperature air loop, low temperature air with room temperature flows through filter, flow control valve, flow meter and then enter the heat exchanger. The flow rate of low temperature air can be controlled using flow meter.

The back pressure of both loops was controlled by two different electromagnetic valve, respectively. The air in high temperature loop flows out the heat exchanger and then enters a water-cooled heat exchanger to reduce temperature. The air in low temperature loop from the heat exchanger is exhausted directly to atmosphere due to low temperature. What's more, in the experiments, the whole test section was covered by heat insulation materials with thermal conductivity of less than 0.012 W/(m K) to reduce heat loss.

3.2. Test section

As illustrated in Fig. 3, the air-air heat exchanger was designed carefully in order to reduce the size and mass. The heat exchanger was made of stainless steel type 321 with 175 mm in length, 145 mm in width and 140 mm in height, which can be compacted enough to be installed into the bypass of the aero engine. Tubes with outer diameter of 5 mm and inner diameter of 4.4 mm were selected, and each tube has six passes with 625.6 mm in length. The length, width and height of the inlet and outlet headers are 135 mm, 32 mm and 32 mm, respectively. The total weight of heat exchanger is 2.04 kg.

The detailed structure of the designed heat exchanger was listed in Fig. 4.

Fig. 4(a) shows the detailed dimensions of tube. In the current work, the tube bending radius is larger than 6 mm, which leads to a big distance between adjacent tubes. In order to make the heat exchanger more compact, four tubes are arranged in parallel. As shown in Fig. 4(b), four tubes are arranged in a row with 10 rows in total. It is worth to mention that, in order to avoid the interference between the tubes, four adjacent tubes are bended in opposite directions. The bended angle between the tube and the gravity line is 8°. In this way all the straight section can be arranged in the same level. Using this arrangement, the heat exchanger can be more compact, and the heat transfer area in unit volume can be increased to the maximum value. In addition, it is useful to calculate the flow resistance and heat transfer ability of the heat exchanger.

All 40 tubes were fabricated and arranged firstly. After that, two groups of support plate were installed into the interspace between tubes to strengthen the firmness of the tubes. At the same time, the inlet and outlet section of the tubes were inserted into the headers together. Then the liquid solder was coated on

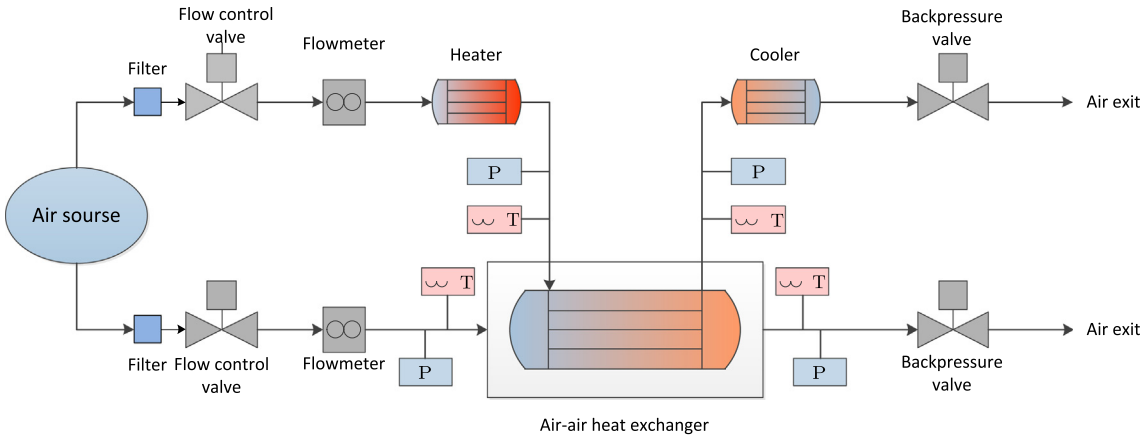

Fig. 2. Schematic of experiment system.

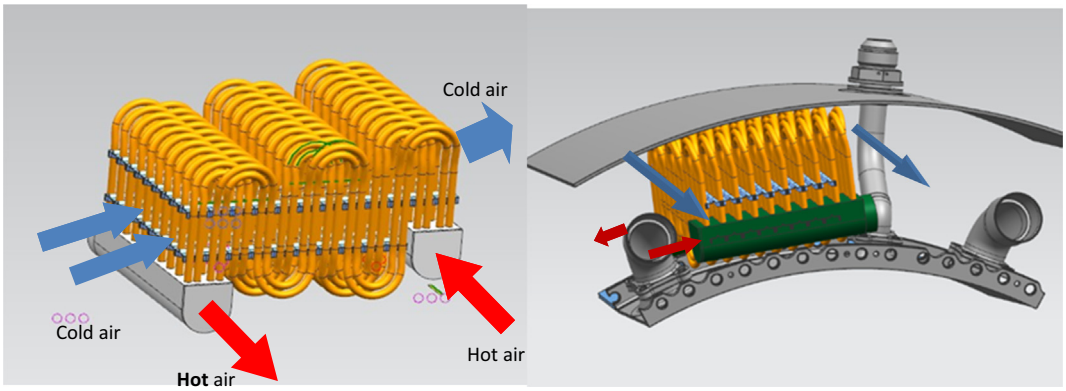

Fig. 3. Design diagram of heat exchanger.

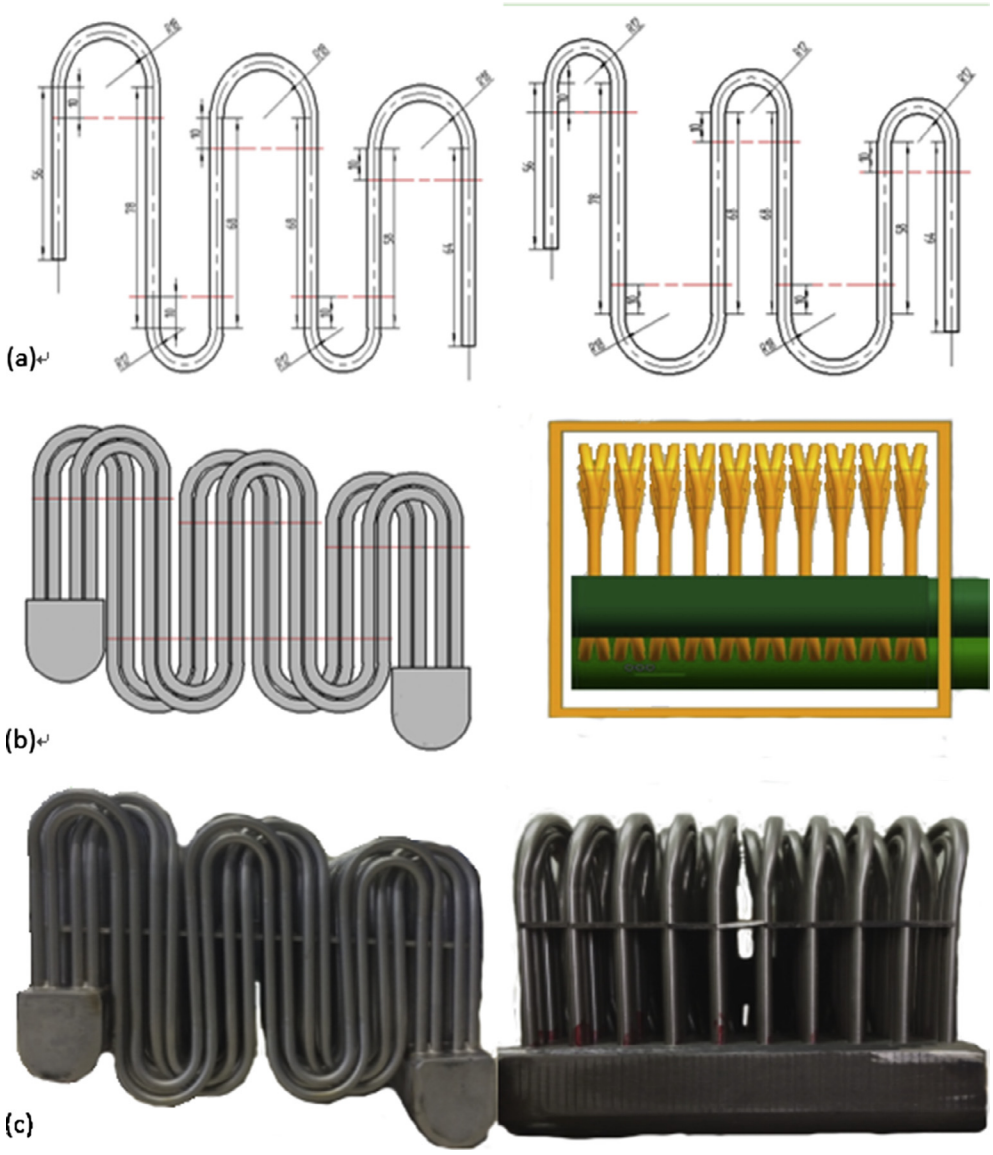

Fig. 4. Detailed structure of heat exchanger.

Table 2
Uncertainty of the direct measurements.

Direct measurement	Measuring instrument	Measure uncertainty
Absolute pressure	Rosemount pressure transmitter	0.25%
Pressure drop	Rosemount pressure transmitter	0.04%
Mass flow rate	Thermal flow meter (hot side) Orifice flow meter (cold side)	0.5%
Temperature	K type sheathed thermocouple	0.6 K
Tube diameter	Vernier caliper	0.02 mm
Length	Tape	0.1 mm

the contact surfaces between the support plates and the headers as well as the tubes. At last, the whole heat exchanger was sent to a high temperature vacuum braze furnace, in which the heat exchanger was brazed. Fig. 4(c) shows the photos of the completed heat exchanger.

3.3. Uncertainty analysis

Table 2 shows the experimental uncertainty under the direct measurements.

By using the error propagation under non-linear form [25], the uncertainty of heat transfer coefficient can be calculated using following equations:

$$\frac{\Delta K}{K}=\sqrt{\left(\frac{\Delta m}{m}\right)^2+\frac{\Delta T_{in}^2+\Delta T_{out}^2}{(T_{in}-T_{out})^2}+\frac{\left(\frac{\partial \Delta T_m}{\partial \Delta T_{max}}\Delta(\Delta T_{max})\right)^2+\left(\frac{\partial \Delta T_m}{\partial \Delta T_{min}}\Delta(\Delta T_{min})\right)^2}{\Delta T_m^2}} \quad (5)$$

Taking the individual uncertainties of the measurements into Eq. (5), the combined uncertainty is estimated to be 6.69% in all experimental regions.

4. Results and discussion

As previously mentioned, the air at room temperature and the heated air were used to simulate the bypass air and HPC bleed air in an aircraft engine, respectively. Experiments were performed to test the overall flow resistance and heat transfer of the heat exchanger. In the experiments, the temperature and flow rates for high temperature air and low temperature air changes respectively. In addition, repeatability tests were made to investigate the effect of the heat exchanger processing.

4.1. Flow resistance

Fig. 5 shows the pressure loss on both hot side and cold side of the heat exchanger at different mass flow rates. In this figure, it can be seen clearly that the flow resistance increases with the increase of the mass flow rate for both cold side and hot side. However, the cold side flow resistance is very low, whereas the flow resistance on the hot side is much higher. The reason could be due to the fact that the hot side tube is thinner and the flow channel is more complex, which will increase the flow resistance. Meanwhile, the cold side flow resistance is lower since the tube are in aligned arrangement. Actually, the maximum of the hot side mass flow is less than 0.075 kg/s in practical application, as a consequence, the pressure loss could be less than 25%.

Fig. 6 presents the divergence between the predicting pressure loss and experimental results at six different mass flow rates for both hot air side and cold air side, respectively. For the hot air side, the percentage of the pressure loss error is defined as:

$$\text{Hot side pressure loss error}=\frac{|\Delta p_{h,exp}-\Delta p_{h,ver}|}{\Delta p_{h,ver}}*100\% \quad (6)$$

Similarly, the percentage of the pressure loss error for the cold side is defined as:

$$\text{Cold side pressure loss error}=\frac{|\Delta p_{c,exp}-\Delta p_{c,ver}|}{\Delta p_{c,ver}}*100\% \quad (7)$$

Fig. 6(a) shows that the error for the hot air side is lower than 15% for all seven mass flow rates. These error may be related to the uncertainties associated with the several instruments such as flow meters and sheathed thermocouples. Meanwhile, the air flow rates cannot be recorded accurately due to the fluctuations even if the flow rates of both side are the averaged value by time. Fig. 6(b) shows that the maximum difference between the predicted value and experimental data is about 30% at different mass flow rates. The big error is also related to the very small pressure drop of the cold side because the relative error by Rosemount pressure transmitter in experiments is larger in the case of that the absolute error is constant. Despite this, the error value at different mass flow rates in Fig. 6 is close to each other, which still support the overall accuracy of the heat exchanger design and verification method.

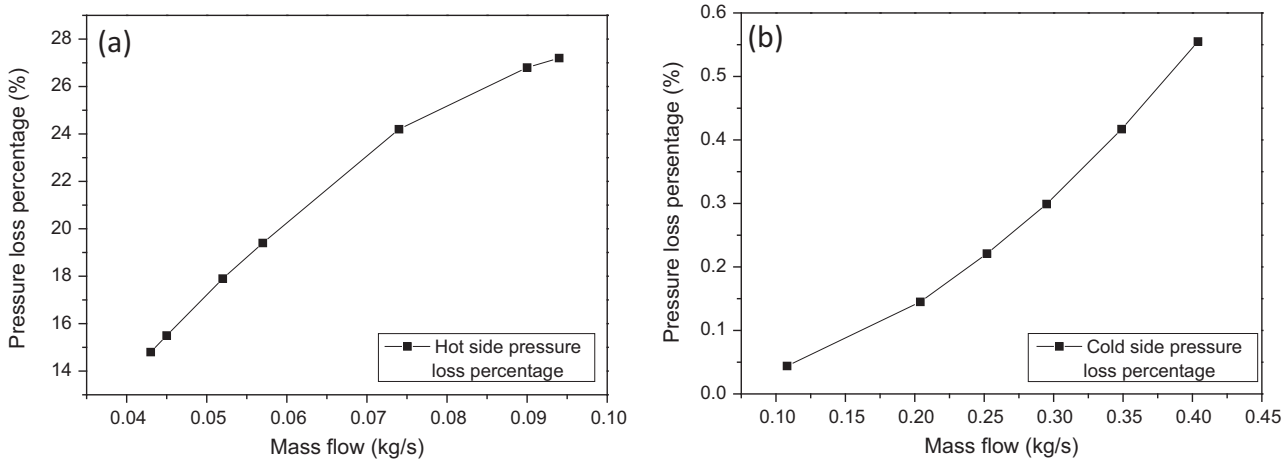

Fig. 5. Pressure loss of (a) hot side and (b) cold side in different mass flow.

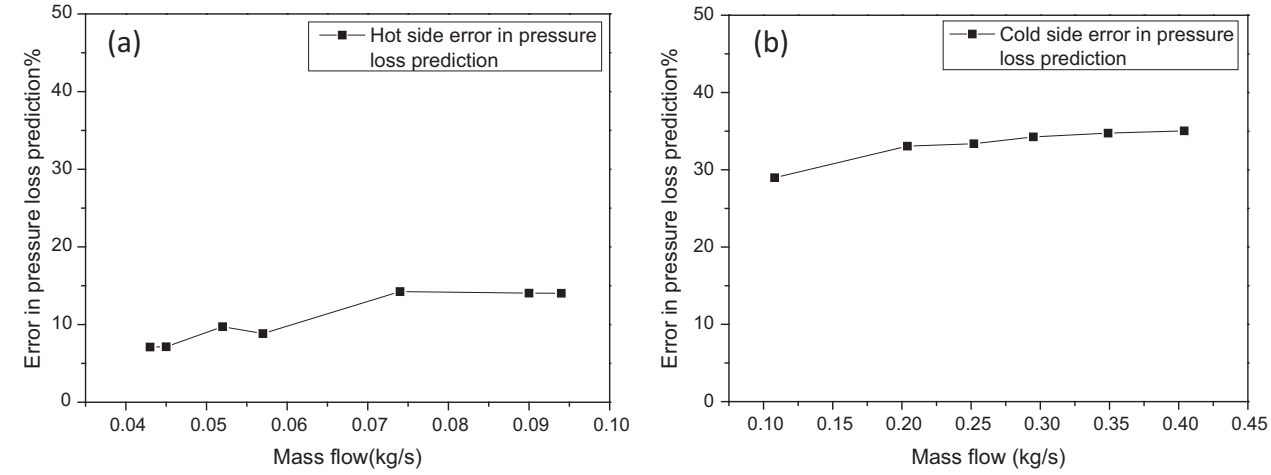

Fig. 6. Error of pressure loss prediction of (a) hot side and (b) cold side in different mass flow.

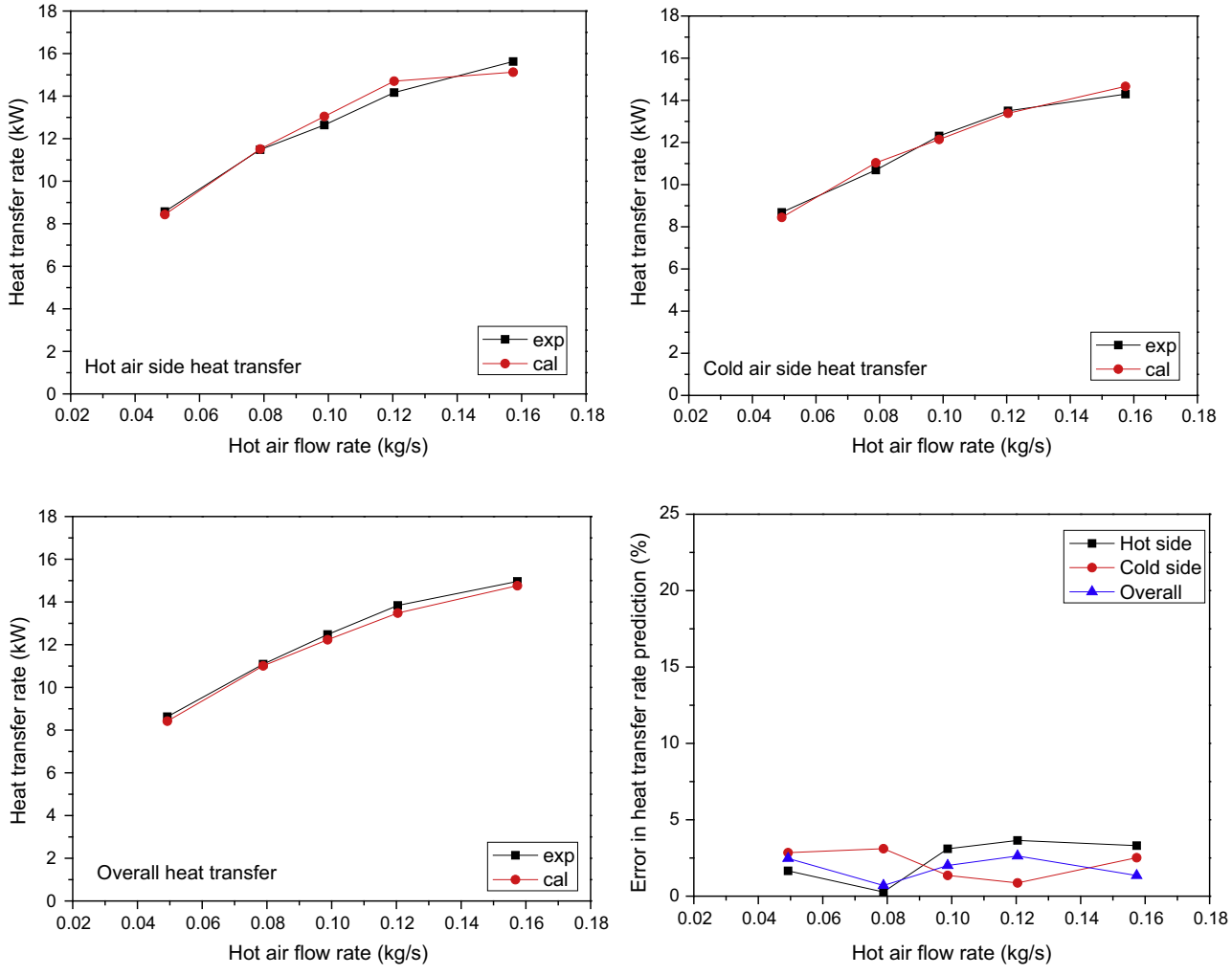

Fig. 7. Heat transfer rate comparison between calculation and experiments in the cold air flow rate of 0.4 kg/s.

4.2. Heat transfer

The heat transfer rates of the heat exchanger are measured and calculated for the cold and hot side, respectively, as Eq. (1).The overall heat transfer rates are also experimentally measured and calculated by Eq. (4).

In these experiments, the hot side flow rates range from 0.05 kg/s to 0.2 kg/s, while the flow rates on the cold side changes from 0.1 kg/s to 0.6 kg/s. As illustrated in Fig. 7, the predicted and experimental heat transfer rates were calculated and compared with each other for both hot side and cold side respectively. At the same time, the cold air flow rate keeps constant at

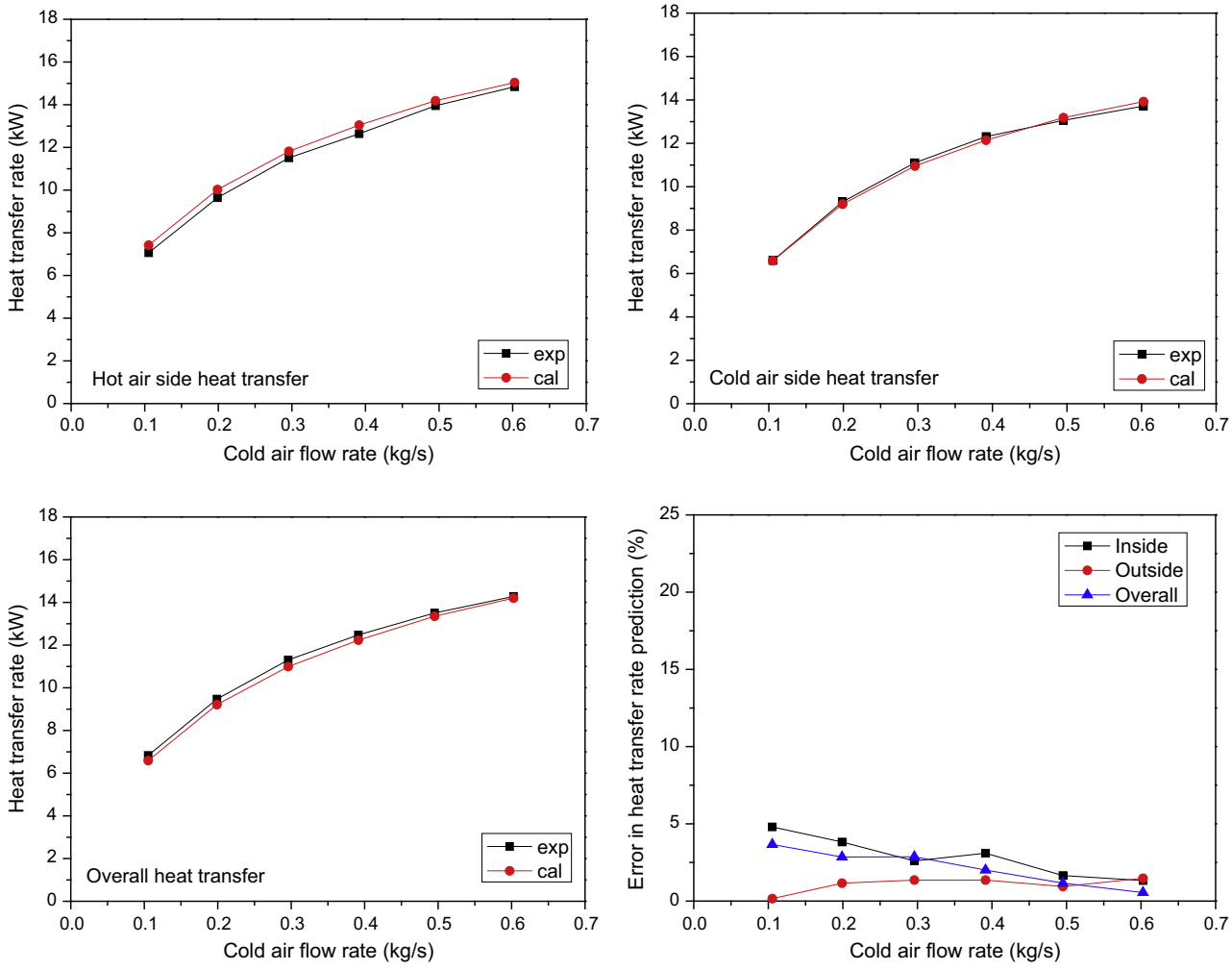

Fig. 8. Heat transfer rate comparison between calculation and experiments in the hot air flow rate of 0.1 kg/s.

0.4 kg/s. It is clearly observed that the hot side, cold side and overall heat transfer rate all increase with the increase of the hot air flow rate. In addition, for the three different heat transfer, the error in heat transfer rate prediction is all less than 4%. Fig. 8 compared the same comments with Fig. 7 in the hot air flow rate of 0.1 kg/s. Heat transfer rate also increases with the increase of the cold air flow rate and heat transfer rate prediction error is less than 5%. The results show good agreement in a wide range of mass flow rates for both hot side and cold side quantitatively and qualitatively.

The all 30 calculated and experimental heat transfer rates were compared in Fig. 9. The deviation between the experimental average heat transfer rate and calculated values for the cold air side, hot air side and overall heat exchanger is 3.06%, 2.04% and 2.10%, respectively. What's more, when predicting hot air side heat transfer rates, 86.7% points in 30 points are in the 5% error band, and when predicting cold air side and overall heat transfer rates, the proportion is even higher, which is up to 96.7% in 30 points in 5% error band.

These results demonstrated that the design method in this paper as a tool for heat transfer performance prediction of compact air-air heat exchangers is effective.

4.3. Repeatability

Considering the effect of the machining error, repeatability test were conducted in the paper. Two air-air heat exchanger with same scale and other parameters were manufactured and tested under the hot side flow rate of 0.08 kg/s and 0.1 kg/s and cold side from 0.2 kg/s to 0.4 kg/s, respectively. Fig. 10 exhibited the divergence in heat transfer rate prediction with six different working conditions. The results showed that the maximum influence of the machining on heat transfer rates is less than 10.8%, which is acceptable in engineering practice.

4.4. Outside heat transfer coefficient empirical relationship

In the design of the heat exchanger, the determination of the outside heat transfer coefficient empirical relationship is one of the most important issues. However, no empirical relationship can be used in all cases. For instance, the heat transfer coefficient empirical relationship used in this paper is Zhukauskas empirical relationship. But the Zhukauskas empirical relationship is developed for the case of the fluid flowing across the straight tube row. It is not suitable for the snake tubes which was applied in this paper since the snake tubes have some bent section. This means that the Zhukauskas relationship cannot be applied to the heat transfer pattern of the snake tube appropriately. On the other hand, the structure and geometry are always changed with different condition in application, so it is important to develop an empirical relationship for the snake tube heat exchanger.

Because the heat exchanger applied in aero engine is compact, it is difficult to measure the wall temperature of the tubes. As a consequence, it is hard to calculate the heat transfer coefficient

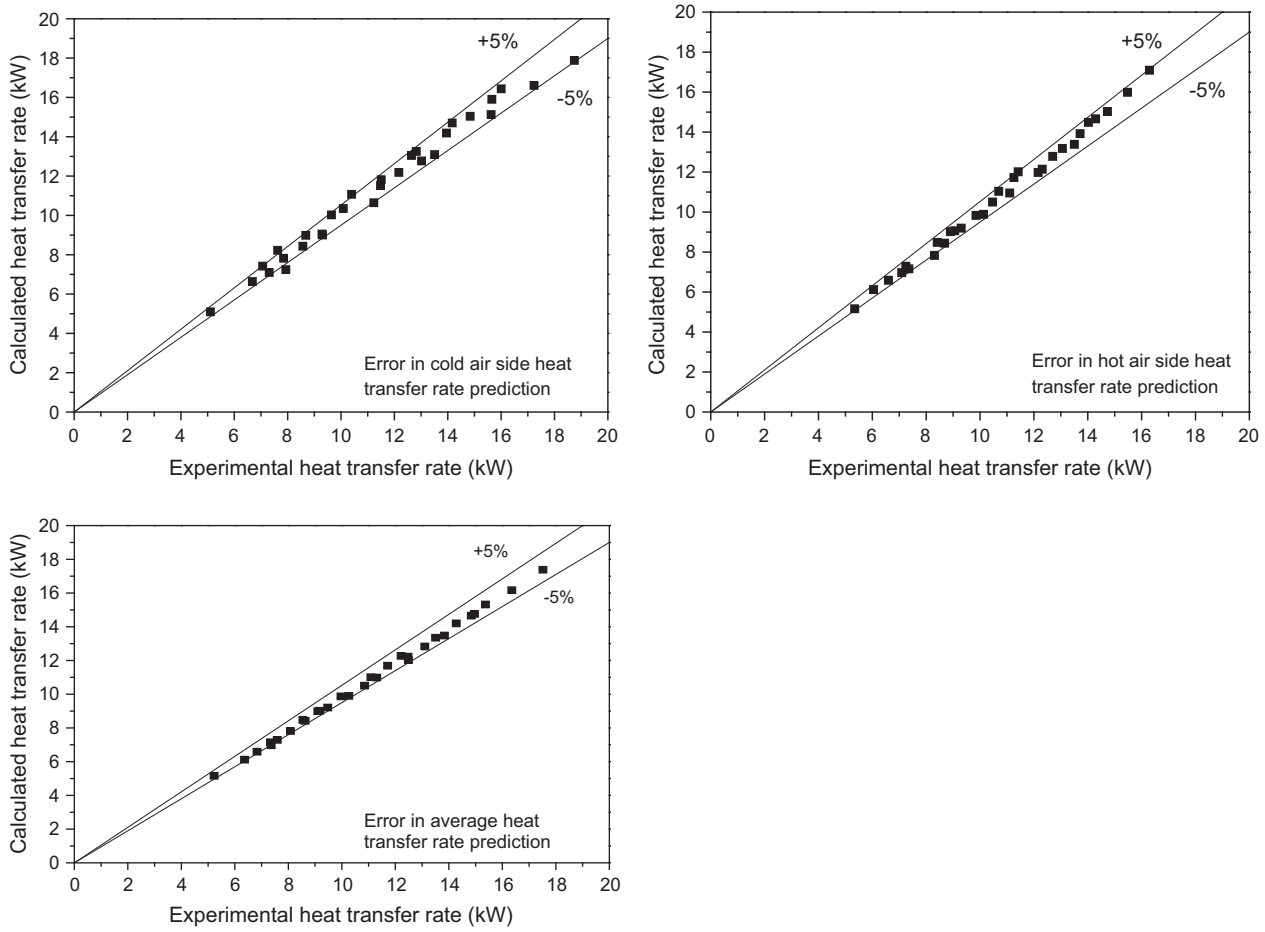

Fig. 9. Comparison of the experimental and calculated heat transfer prediction.

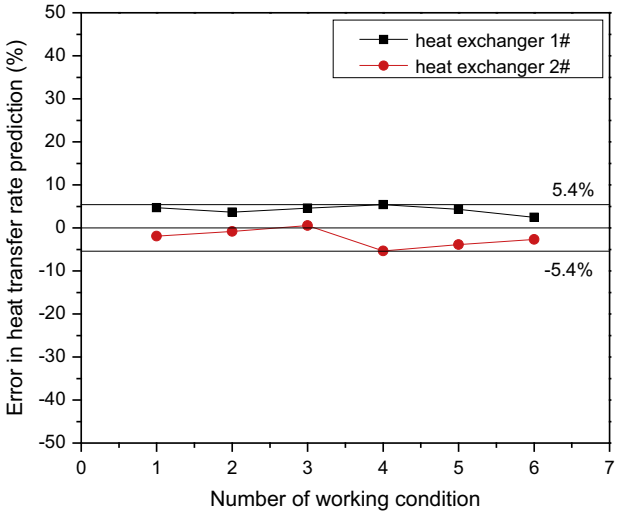

Fig. 10. Comparison of heat exchangers with same scale.

between the wall and the outside air. In the current work, the so-called Wilson plot method was introduced to determine the heat transfer relationships for either side of a heat exchanger based on the measurements of the heat transfer rate and overall temperature difference between the two fluids. This could be easier to measure the wall temperature along flow direction.

By using Wilson plot method, the form of the relationship should be determined firstly. Reference to Zhukauskas relationship, the relationship of the heat exchanger can be defined as:

$$Nu_o = CRe^n Pr_f^m \left(\frac{Pr_f}{Pr_w}\right)^p \tag{8}$$

where p and m can be determined as 0.25 and 0.36, respectively, with a large Re number range from 1 to 2×10^6 because the temperature influence Pr number of air little. The values of C and n in the relationship will be determined below.

In the heat transfer process, the total thermal resistance is defined as follow:

$$R_t = \frac{1}{K} = \frac{d}{\lambda * Nu} = R_w + R_i + R_o + R_s \tag{9}$$

Replace R_o and R_i with $\frac{d}{\lambda * Nu_o}$ and $\frac{d}{\lambda * Nu_i}$, respectively, R_t can be rewritten as:

$$R_t = \frac{1}{K} = R_w + R_s + \frac{d_i}{\lambda * Nu_i}, + \frac{d_o}{\lambda * Nu_o} \tag{10}$$

Since the heat exchanger is newly fabricated, the fouling thermal resistance R_s can be considered as zero. The thermal resistance of the tube wall R_w and Nu_i can calculated by tube wall thickness and Re_i, respectively.

Eq. (8) can be rewritten as:

$$\frac{Nu_o}{Pr_f^m \left(\frac{Pr_f}{Pr_w}\right)^p} = CRe_o^n \tag{11}$$

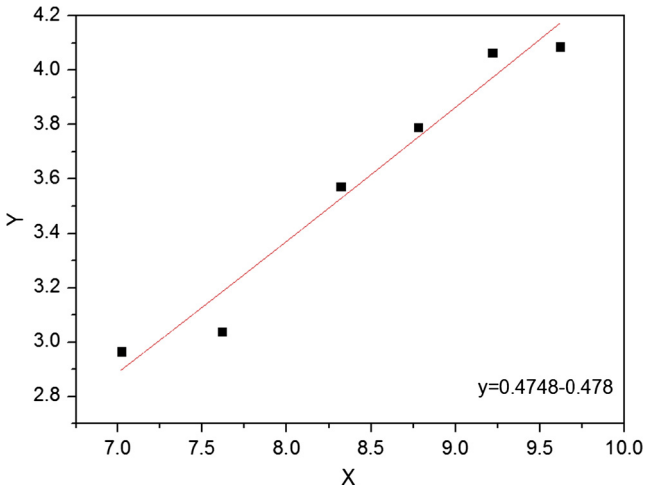

Fig. 11. The line fitted by using Wilson plot method.

and

$$\ln\left(\frac{Nu_o}{Pr_f^m\left(\frac{Pr_f}{Pr_w}\right)^p}\right) = \ln C + n\ln Re_o \tag{12}$$

where the unknown Re number can be easily calculated by m_c and μ.

Eq. (12) can be rearranged as

$$\ln\left(\frac{d_0}{\left(\frac{\lambda}{K}-\lambda R_w-\frac{d_i}{Nu_i}\right)Pr_f^m\left(\frac{Pr_f}{Pr_w}\right)^p}\right) = \ln C + n\ln Re_o \tag{13}$$

which can be deformed as:

$$Y = a + b * X \tag{14}$$

where $Y = \ln\left(\frac{d_0}{\left(\frac{\lambda}{K}-\lambda R_w-\frac{d_i}{Nu_i}\right)Pr_f^m\left(\frac{Pr_f}{Pr_w}\right)^p}\right)$, $X = \ln Re_o$, $a = \ln C$, $b = n$

Based on the above discussion, Eq. (13) reduces into a linear equation. In this equation, a is intercept and b is slope.

In the experiments, when the value of X and the corresponding value of Y is calculated, the relationship between X and Y can be described. The relationship between X and Y can be obtained by fitting the data for X and Y. Then, the values of C and n can be determined accordingly.

Fig. 11 exhibits the line fitted by using Wilson plot method.

The modified outside heat transfer coefficient empirical relationship for six-pass snake tube heat exchanger is shown as follow:

$$Nu = 0.62Re^{0.4748}Pr_f^{0.36}\left(\frac{Pr_f}{Pr_w}\right)^{0.25} \tag{15}$$

where $0.67 < Pr < 0.7$ and $1000 < Re < 15{,}000$.

The empirical relationship can be a reference for the design of heat exchanger with similar structure.

There are two requirements should be satisfied when using Wilson plot method. One of the requirements is that the fouling thermal resistance should be zero or able to be calculated exactly; the other is that the inside heat transfer coefficient empirical relationship should be known. Both the two conditions were satisfied in the experiments.

5. Conclusions

This paper mainly investigated the design, verification and performance assessment of a novel air-air heat exchanger intended for potential application in gas turbine engines. The LMTD method is used in the heat exchanger design and verification .The comparison between the calculated results and experimental data was carried out. Analysis of the experimental and theoretical results may lead to the following main conclusions:

(1) A new compact cross-flow air-air heat exchanger with stainless-steel-made snake tube was designed and optimized, which is both light in weight and with strong heat transfer capability.
(2) Comparisons between calculation and experiments show good agreement in both pressure losses and heat transfer rates. All these proves the LMTD method is reliable enough for designing the heat exchanger and predicting the performance
(3) Wilson plot method is used in modifying the outside heat transfer coefficient empirical relationship, and an empirical relationship for outside heat transfer coefficient is developed, which can be a reference for the design of heat exchanger with similar structure.

References

[1] Y.J. Kim, S.M. Kim, Influence of shaped injection holes on turbine blade leading edge film cooling, Int. J. Heat Mass Transf. 47 (2004) 245–256.
[2] V.K. Garg, Modeling film-coolant flow characteristics at the exit of shower-head holes, Int. J. Heat Fluid Flow 22 (2001) 134–142.
[3] C.H.N. Yuen, R.F. Martinez-Botas, Film cooling characteristics of a single round hole at various streamwise angles in a crossflow: part I effectiveness, Int. J. Heat Mass Transf. 46 (2003) 221–235.
[4] J.C. Han, S. Dutta, S.V. Ekkad, Gas Turbine Heat Transfer and Cooling Technology, Taylor & Francis, New York, 2000.
[5] P. Martini, A. Schulz, H.J. Bauer, Film cooling effectiveness and heat transfer on the trailing edge cutback of gas turbine airfoils with various internal cooling designs, J. Turbomach. Trans. ASME 128 (2006) 196–205.
[6] H. Huang, L.J. Spadaccini, D.R. Sobel, Fuel-cooled thermal management for advanced aeroengines, Trans. ASME 126 (2004) 284–293.
[7] O. Altin, S. Eser, Analysis of carboneceous deposits from thermal stressing of a JP-8 fuel on superalloy foils in a flow reactor, Ind. Eng. Chem. Res. 40 (2) (2001) 589–595.
[8] O. Altin, S. Eser, Analysis of solid deposits from thermal stressing of a JP-8 fuel on different tube surfaces in a flow reactor, Ind. Eng. Chem. Res. 40 (2) (2001) 596–603.
[9] D.L. Linne, M.L. Meyer, T. Edwards, D.A. Eitman, Evaluation of heat transfer and thermal stability of supercritical JP-7 fuel, NASA Technical Memorandum 107485, AIAA-97-3041.
[10] W. Gao, H.S. Liang, Q.H. Xu, Y.Z. Lin, C.J. Sung, Injection of supercritical aviation kerosene fuel into quiescent atmospheric environment, in: 45thAIAA/ASME/SAE/ASEE Joint Propulsion Conference & Exhibit, 2–5 August 2009, Denver, Colorado, AIAA 2009–4927.
[11] F.Q. Zhong, X.J. Fan, G. Yu, J.G. Li, C.J. Sung, Heat transfer of aviation kerosene at supercritical conditions, J. Thermophys. Heat Transfer 23 (3) (2009) 543–550.
[12] Y.Q. Kong, L.J. Yang, X.Z. Du, Y.P. Yang, Air-side flow and heat transfer characteristics of flat and slotted finned tube bundles with various tube pitches, Int. J. Heat Mass Transf. 99 (2016) 357–371.
[13] X. Liu, J. Yu, G. Yan, A numerical study on the air-side heat transfer of perforated finned-tube heat exchangers with large fin pitches, Int. J. Heat Mass Transf. 100 (2016) 199–207.
[14] L. Vafajoo, K. Moradifar, S.M. Hosseini, B.H. Salman, Mathematical modelling of turbulent flow for flue gas–air Chevron type plate heat exchangers, Int. J. Heat Mass Transf. 97 (2016) 596–602.
[15] L.Z. Zhang, Flow maldistribution and thermal performance deterioration in a cross-flow air to air heat exchanger with plate-fin cores, Int. J. Heat Mass Transf. 52 (19) (2009) 4500–4509.
[16] J.V. Vargas, A. Bejan, Thermodynamic optimization of finned crossflow heat exchangers for aircraft environmental control systems, Int. J. Heat Fluid Flow 22 (6) (2001) 657–665.
[17] S. Boggia, K. Rud, Intercooled recuperated gas turbine engine concept, AIAA Paper, (2005–4192), 2005.
[18] D. Missirlis, K. Yakinthos, A. Palikaras, K. Katheder, A. Goulas, Experimental and numerical investigation of the flow field through a heat exchanger for aero-engine applications, Int. J. Heat Fluid Flow 26 (3) (2005), 440–458.1.

[19] K. Yakinthos, D. Missirlis, A. Palikaras, P. Storm, B. Simon, A. Goulas, Optimization of the design of recuperative heat exchangers in the exhaust nozzle of an aero engine, Appl. Math. Model. 31 (11) (2007) 2524–2541.
[20] C. Albanakis, K. Yakinthos, K. Kritikos, D. Missirlis, A. Goulas, P. Storm, The effect of heat transfer on the pressure drop through a heat exchanger for aero engine applications, Appl. Therm. Eng. 29 (4) (2009) 634–644.
[21] J.M. Kay, R.M. Nedderman, Fluid mechanics and transfer processes, CUP Archive, 1985.
[22] S.A. Klein, Engineering Equation Solver (EES), F-Chart Software, Madison, WI.
[23] Mei Zhong Shi, Zhong Zheng Wang, Principle and Design of Heat Exchangers, fifth ed., Southeast University Press, Nanjing, China, 1989 (in Chinese).
[24] Yang Shiming, Tao Wenquan, Heat Transfer, Fourth ed., Higher Education Press, Beijing, China, 1998 (in Chinese).
[25] H.H. Ku, Notes on the use of propagation of error formulas, J. Res. Nat. Bur. Stand. 70 (4) (1966).